Author Manuscript

Author Manuscript

Author Manuscript

Author Manuscript

HHS Public Access

Author manuscript

Adv Healthc Mater. Author manuscript; available in PMC 2018 June 01.

Published in final edited form as:

Adv Healthc Mater. 2017 June ; 6(12): . doi:10.1002/adhm.201601451.

Extrusion Bioprinting of Shear-Thinning Gelatin Methacryloyl Bioinks

Wanjun Liu,
Biomaterials Innovation Research Center, Division of Engineering in Medicine, Brigham and Women's Hospital, Harvard Medical School, Cambridge, MA 02139, USA

Harvard-MIT Division of Health Sciences and Technology, Massachusetts Institute of Technology, Cambridge, MA 02139, USA

Key Laboratory of Textile Science and Technology, College of Textiles, Donghua University, Shanghai 201620, China

Marcel A. Heinrich,
Biomaterials Innovation Research Center, Division of Engineering in Medicine, Brigham and Women's Hospital, Harvard Medical School, Cambridge, MA 02139, USA

Harvard-MIT Division of Health Sciences and Technology, Massachusetts Institute of Technology, Cambridge, MA 02139, USA

MIRA Institute of Biomedical Technology and Technical Medicine, Department of Developmental BioEngineering, University of Twente, Enschede 7500AE, Netherlands

Yixiao Zhou,
Biomaterials Innovation Research Center, Division of Engineering in Medicine, Brigham and Women's Hospital, Harvard Medical School, Cambridge, MA 02139, USA

Harvard-MIT Division of Health Sciences and Technology, Massachusetts Institute of Technology, Cambridge, MA 02139, USA

Prof. Ali Akpek,
Biomaterials Innovation Research Center, Division of Engineering in Medicine, Brigham and Women's Hospital, Harvard Medical School, Cambridge, MA 02139, USA

Harvard-MIT Division of Health Sciences and Technology, Massachusetts Institute of Technology, Cambridge, MA 02139, USA

Department of Biomedical Engineering, Istanbul Yeni Yuzyil University, Istanbul 34010, Turkey

Dr. Ning Hu,
Biomaterials Innovation Research Center, Division of Engineering in Medicine, Brigham and Women's Hospital, Harvard Medical School, Cambridge, MA 02139, USA

Correspondence to: Ali Khademhosseini; Yu Shrike Zhang.

Supporting Information

Supporting Information is available from the Wiley Online Library or from the author.

Author Manuscript Author Manuscript Author Manuscript Author Manuscript

Harvard-MIT Division of Health Sciences and Technology, Massachusetts Institute of Technology, Cambridge, MA 02139, USA

Prof. Xiao Liu,
Biomaterials Innovation Research Center, Division of Engineering in Medicine, Brigham and Women's Hospital, Harvard Medical School, Cambridge, MA 02139, USA

Harvard-MIT Division of Health Sciences and Technology, Massachusetts Institute of Technology, Cambridge, MA 02139, USA

Key Laboratory for Biomechanics and Mechanobiology of the Ministry of Education, School of Biological Science and Medical Engineering, Beihang University, Beijing 100191, China

Xiaofei Guan,
Biomaterials Innovation Research Center, Division of Engineering in Medicine, Brigham and Women's Hospital, Harvard Medical School, Cambridge, MA 02139, USA

Harvard-MIT Division of Health Sciences and Technology, Massachusetts Institute of Technology, Cambridge, MA 02139, USA

Zhe Zhong,
Biomaterials Innovation Research Center, Division of Engineering in Medicine, Brigham and Women's Hospital, Harvard Medical School, Cambridge, MA 02139, USA

Harvard-MIT Division of Health Sciences and Technology, Massachusetts Institute of Technology, Cambridge, MA 02139, USA

Prof. Xiangyu Jin,
Key Laboratory of Textile Science and Technology, College of Textiles, Donghua University, Shanghai 201620, China

Prof. Ali Khademhosseini, and
Biomaterials Innovation Research Center, Division of Engineering in Medicine, Brigham and Women's Hospital, Harvard Medical School, Cambridge, MA 02139, USA

Harvard-MIT Division of Health Sciences and Technology, Massachusetts Institute of Technology, Cambridge, MA 02139, USA

Wyss Institute for Biologically Inspired Engineering, Harvard University, Boston, MA 02115, USA

Department of Bioindustrial Technologies, College of Animal Bioscience and Technology, Konkuk University, Seoul 143-701, Republic of Korea

Dr. Yu Shrike Zhang
Biomaterials Innovation Research Center, Division of Engineering in Medicine, Brigham and Women's Hospital, Harvard Medical School, Cambridge, MA 02139, USA

Harvard-MIT Division of Health Sciences and Technology, Massachusetts Institute of Technology, Cambridge, MA 02139, USA

Wyss Institute for Biologically Inspired Engineering, Harvard University, Boston, MA 02115, USA

Abstract

Author Manuscript Author Manuscript Author Manuscript Author Manuscript

Bioprinting is an emerging technique for the fabrication of three-dimensional (3D) cell-laden constructs. However, the progress for generating a 3D complex physiological microenvironment has been hampered by a lack of advanced cell-responsive bioinks that enable bioprinting with high structural fidelity, particularly in the case of extrusion-based bioprinting. Herein, we report a novel strategy to directly bioprint cell-laden constructs using bioinks made of gelatin methacryloyl (GelMA) physical gels (GPGs). Attributed to their shear-thinning and self-healing properties, the GPG bioinks could retain the shape and form integral structures after deposition, allowing for subsequent UV crosslinking for permanent stabilization. We showed the structural fidelity by bioprinting various 3D structures that are typically challenging to fabricate using conventional bioinks under extrusion modes. Moreover, the use of the GPG bioinks enabled direct bioprinting of highly porous and soft constructs at relatively low concentrations (down to 3%) of GelMA. We also demonstrated that the bioprinted constructs not only permitted cell survival but also enhanced cell proliferation as well as spreading at lower concentrations of the GPG bioinks. We believe our strategy of bioprinting will provide many opportunities in convenient fabrication of 3D cell-laden constructs for applications in tissue engineering, regenerative medicine, and pharmaceutical screening.

Keywords

bioprinting; gelatin methacryloyl (GelMA); cell-laden; hydrogel; tissue engineering

1. Introduction

Generation of biomimetic three-dimensional (3D) tissue-like structures is in increasing demand for applications in tissue engineering, regenerative medicine, and pharmaceutical screening[1, 2]. To date, many technologies including bioprinting, photolithography, and electrospinning[3] have been adopted for the fabrication of 3D tissue constructs. Among them, bioprinting shows great potential as it is able to provide precise spatial manipulation of living cells and functional components such as extracellular matrix (ECM) and bioactive molecules, giving the possibility of recapitulating the complex physiological microenvironment of 3D tissues and organs. Common bioprinting strategies include inkjet printing, extrusion printing, laser-assisted forward transfer, and stereolithography[2, 4, 5, 6]. While they all possess advantages and disadvantages, extrusion-based bioprinting has become one of the most widely used modalities due to its relatively low cost and compatibility with various bioinks[7].

Hydrogel-based bioinks encapsulating living cells and bioactive components are commonly used for bioprinting[8]. So far, a range of hydrogels including collagen/gelatin[9], gelatin methacryloyl (GelMA)[10, 11], alginate[12, 13], fibrin[14], hyaluronic acid (HA)[15], poly(ethylene glycol) diacrylate (PEGDA)[16], poly(ethylene glycol) dimethacrylate (PEGDMA)[17], and pluronic[18, 19] have been demonstrated their use in extrusion-based bioprinting, but none of these formulations have been able to fulfill all the requirements of direct deposition of free-standing cell-favorable structures due to their limited printability when used alone[9, 14], inferior mechanical properties[11, 17], slow gelation[10], or insufficient cytocompatibility[16–18, 20]. Therefore, hybrid hydrogel formulations (e.g. alginate, PEGDA,

Author Manuscript Author Manuscript Author Manuscript Author Manuscript

collagen, and fibrin) have been adopted for extrusion-based bioprinting[12, 20, 21], but the mechanical properties still rarely satisfy the requirements for bioprinting while at the same time maintaining normal cell activities.

Among different types of bioinks, GelMA bioinks hold great promise attributed to their superior cytocompatibility and broadly tunable physical properties[22, 23]. Although stereolithography is a promising technology for high-resolution bioprinting of GelMA bioinks[6, 24], the bioprinter setup is usually complex. Extrusion bioprinting is so far the most widely used strategy for GelMA bioprinting. However, challenges still remain for direct extrusion bioprinting of GelMA bioinks. For example, the few previous reports using GelMA-based bioinks could only use them at concentrations of higher than 7%, which was limited by the bioprinting strategies that required localized gelation and photocrosslinking[10, 11, 25]. These overly high concentrations of GelMA bioinks resulted in limited cell activities in the bioprinted constructs due to the relatively high stiffness of the crosslinked constructs. On the other hand, we have recently designed a microfluidic printhead for direct bioprinting of GelMA constructs using alginate/GelMA as the composite bioink[20, 26], where the alginate component was selectively removed after bioprinting to leave only GelMA. Nevertheless, this strategy could only deposit microfibrous structures carried by the outer crosslinking sheath flow containing $CaCl_2$, and thus smooth integration of the bioprinted microfibers into a single tissue unit cannot be achieved. Moreover, an embedded bioprinting technique has been recently developed, which allows for freeform deposition of soft hydrogel bioinks in supporting matrices followed by removal of the matrices to retrieve the bioprinted structures[27]. However, such process is relatively complex requiring multi-step procedures. Therefore, it remains a vital challenge to develop novel bioinks that can enable the direct bioprinting of 3D cell-laden constructs with a high structural fidelity and proper cell activities integration, or novel strategies that enable such outcome using existing bioinks.

Here we report a new strategy that allows for direct bioprinting of 3D cell-laden pure GelMA constructs with high structural fidelity and enhanced bioactivity, by employing GelMA physical gels (GPGs) as the bioinks, achieved through a simple cooling process. Attributed to their shear-thinning and self-healing properties, GPGs did not require localized gelation or crosslinking to enable extrusion bioprinting. As such, the GPG bioinks at relatively low concentrations (down to 3%) could retain their structures and form integral structures that were very soft (~1.8 kPa) upon deposition, facilitating bioprinting of temporally stable structures that could be subsequently subjected to permanent photocrosslinking. In particular, we examined the gelation kinetics of the GelMA solutions for better understanding of the fundamental behaviors of the GPG bioinks. We then investigated the structural fidelity by printing various 3D objects using the GPG bioinks. We finally examined the cell viability as well as their proliferation and spreading in the GelMA constructs formed by bioprinting of the GPG bioinks.

Author Manuscript Author Manuscript Author Manuscript Author Manuscript

2. Results and Discussion

2.1. The strategy of direct bioprinting of the GPG bioinks

Owing to the presence of intrinsic arginine-glycine-aspartate (RGD) sequences, GelMA possesses superior biological properties, making it an important hydrogel for applications directly involving cells[22, 23, 28, 29]. The GelMA solution is liquid at 37 °C, which becomes a GPG at room temperature (21 °C) or below due to the coil-helix transition aided by intermolecular bonds, showing similar properties with gelatin, its pristine non-methacryloyl substituted form[30]. In addition, the shear-thinning and self-healing properties of the GPG bioinks allow them to be easily ejected from a nozzle without physical clogging, and retain the shape to form integral structures with high structural fidelity after deposition. Furthermore, the GPG bioinks can be permanently stabilized through photocrosslinking due to the presence of methacryloyl groups. These unique properties have made the GPG bioinks ideal candidates for extrusion bioprinting.

Our strategy involves the direct bioprinting of the GPG bioinks into temporally stable structures and subsequent UV crosslinking of the deposited GelMA constructs, endowing them with long-term stability. A modified bioprinter was used in this work for the bioprinting of the GPG bioinks (Fig. 1A). The GPG bioink was prepared through a two-step procedure: *i*) the cells were mixed with the GelMA solution at 37 °C to prepare the GelMA pre-bioink; and *ii*) the GelMA pre-bioink was loaded into a syringe and cooled down to achieve physical gelation into a GPG bioink (Fig. 1B–D).

In comparison with other reported bioprinting approaches[10, 11, 25], direct bioprinting of the GPG bioinks appears benign to cells and simple. By using the GPG bioinks, the bioprinting does not rely on fast chemical crosslinking upon extrusion of the cell-laden bioinks[10], thus allowing for the deposition of bioinks at relatively low concentrations of down to 3%, which is much lower than the reported 7% currently attainable using *in situ* photocrosslinking[10, 11, 25]. It should be noted that such low concentrations would render the bioprinted constructs higher porosity and lower stiffness, which could be useful for applications (e.g., tissue engineering) that require these properties. More importantly, the structural fidelity of the bioprinted constructs could be greatly improved by using the GPG bioinks owing to their distinct shear-thinning and self-healing properties, enabling on-demand deposition of freeform GelMA constructs with both microscale porosity and structural integrity at low concentrations of the bioinks.

2.2. Characterization of the GPG bioinks for direct bioprinting

The gelation kinetics of GelMA solutions is critical to understand the fundamental behaviors of the GPG bioinks. We therefore systematically examined the effect of concentration, temperature and time on their gelation processes. The mechanical spectrum analyses were first conducted at room temperature (21 °C) in the frequency range of 0–100 rad s^{-1}, where all experimental groups showed plateaued moduli, demonstrating the stability of the GPG bioinks (Fig. 2A). Then temperature sweep (oscillation) was conducted by cooling the GelMA solutions from 37 °C to 2 °C at a cooling rate of 5 °C min^{-1} (Fig. 2B). When the temperature was gradually decreased to the gelation temperature (20–30 °C), both G’ and

Author Manuscript Author Manuscript Author Manuscript Author Manuscript

G” for all concentrations of GelMA solutions increased rapidly due to the formation of the GPG bioinks. As the gelation process is time-dependent, time sweep was further performed at 4 °C and 21 °C (the temperatures of cooling and printing processes), respectively (Fig. 2C, D). For all the concentrations and temperatures, G’ and G” increased drastically in the beginning, both of which became constant afterwards. Of note, the final G’ values decreased from 448.7 ± 37.6 Pa to 47.5 ± 12.2 Pa, from 1553.7 ± 100.2 Pa to 147.0 ± 32.4 Pa, and from 1885.3 ± 115.7 Pa to 233.9 ± 6.0 Pa when the cooling temperature was increased from 4 °C to 21 °C for GelMA solutions at concentrations of 3%, 4%, and 5%, respectively (Fig. 2E). Meanwhile, the corresponding final G” values decreased from 3.3 ± 0.3 Pa to 1.2 ± 0.1 Pa, from 10.3 ± 0.5 Pa to 2.4 ± 0.3 Pa, and from 18.1 ± 0.6 to 3.3 ± 0.4 Pa (Fig. 2E). Overall, higher concentration of GelMA solutions resulted in higher G’ and G” values at both 4 °C and 21 °C, while higher temperature led to lower G’ and G” values for all the concentrations of GelMA solutions.

To quantify the gelation process, we also measured the gelation time (Fig. 2F). When the cooling temperature was set as 21 °C, the gelation time for 3%, 4%, and 5% GelMA solutions were 58.0 ± 4.6 min, 29.4 ± 5.9 min, and 22.8 ± 3.5 min, respectively (Fig. S1 and Movie S1). In contrast, the gelation time decreased to less than 16 min for all concentrations of GelMA solutions at the temperature of 4 °C (Fig. S2 and Movie S2). The results indicated that higher concentration and lower temperature led to faster gelation rates. Therefore, we chose to cool GelMA bioinks at 4 °C for 20 min in order to boost the gelation process to obtain GPG bioinks for the subsequent experiments.

The stability of the GPG bioinks for bioprinting was further studied by measuring the evolution of G’ and G” values at 21 °C immediately after cooling the samples at 4 °C for 5 min. Both G’ and G” values decreased but reached steady states in less than 5 min (Fig. 2G), which showed similar values to those achieved by direct gelation at 21 °C (Fig. 2E). In addition, viscosity measurement also showed a similar trend (Fig. 2H), indicating that the cooling process was feasible to accelerate the gelation process without influencing the final properties of the GPG bioinks. We further confirmed that the GPG bioinks exhibited shear-thinning properties. The viscosities of the bioinks increased when the concentration of the GPG bioinks was elevated but all decreased at higher shear rates (Fig. 2I). It should be noted that the GPG bioinks could be smoothly extruded through the bioprinting nozzle, which is also an evidence of the shear-thinning property of the GPG bioinks.

We next examined the influence of feeding rate and nozzle moving speed on the printability using the GPG bioink at an intermediate concentration of 4%. The printability map indicated that a balance between the feeding rate and the nozzle moving speed achieved suitable structural fidelity of the bioprinted constructs (Fig. 3A). Within the printable conditions, the diameter of the deposited filaments decreased from 828.0 ± 148.1 μm to 548.9 ± 200.3 μm when the nozzle moving speed was elevated from 300 mm min^{-1} to 900 mm min^{-1} (feeding rate = 100 μL min^{-1}) (Fig. 3B); alternatively, the diameter increased from 700.0 ± 95.8 μm to 1004.6 ± 88.6 μm as a result of the increase in the feeding rate of the GPG bioink from 50 μL min^{-1} to 150 μL min^{-1} (nozzle moving speed = 500 mm min^{-1}) (Fig. 3C). As an example, GelMA meshes of 9.5 × 9.5 mm^2 with filament spacing of 1.5 mm were obtained, where fluorescence microbeads were encapsulated to facilitate visualization (Fig. 3D–I).

Author Manuscript Author Manuscript Author Manuscript Author Manuscript

The results indicated that the deposited filaments were structurally robust and the boundaries of the filaments were distinct. More importantly, integral slabs could also be obtained by decreasing the spacing between adjacent filaments due to the self-healing property of the GPG bioinks (Fig. 3J–O). Specifically, the healing was complete for the GPG bioinks at concentrations of 3% and 4%, where no distinctive filaments could be recognized from the photographs and fluorescence micrographs (Fig. 3J–M), while the healing was almost complete for the 5% GPG bioink (Fig. 3N, O). Such a high degree of self-healing was not possible with our previous microfluidic bioprinting approach using the hybrid bioink (Fig. S3)[31].

2.3. Bioprinting of 3D constructs

Relative to single-layer structures, the capability of the GPG bioinks to fabricate 3D constructs is more essential to achieve functional bioprinting. The mechanics of the bioprinted cubes (4 layers) with a size of 5 × 5 × 1.6 mm^3 were analyzed for the demonstration of structural fidelity by comparing the compressive modulus of those before and after photocrosslinking (Fig. 4A–C). For the bioprinted constructs without crosslinking, the compression measurements illustrated that Young's modulus was improved from 1.5 ± 0.4 kPa to 1.9 ± 0.3 kPa and 2.6 ± 0.4 kPa when the concentration of the GPG bioinks was increased from 3% to 4% and 5%, respectively (Fig. 4A, C). This trend could also be observed in the samples after crosslinking, but all the three formulations had higher Young's modulus compared to the corresponding uncrosslinked constructs (Fig. 4B, C). It should be noted that, attributed to the shear-thinning and self-healing properties, the GPG bioinks from all the concentrations of 3%, 4%, and 5% could be directly bioprinted into 3D constructs. These bioprinted constructs were stable enough to overcome the gravity, allowing for post-crosslinking to permanently stabilize the structures. In addition, all the uncrosslinked constructs showed sufficient Young's moduli (1.5–2.6 kPa) comparable to the crosslinked constructs bioprinted from 3% GPG bioink (1.8 kPa, Fig. 4C), further indicating that the use of GPG bioinks supported temporary stability after extrusion even without subsequent crosslinking, rendering the high structural fidelity of freshly bioprinted constructs.

The structural fidelity was further validated by direct bioprinting of various 3D architectures. First, a 10-layer cube with a size of 10 × 10 × 4 mm^3 using 4% GPG bioink was successfully bioprinted (Fig. 4D **and** Movie S3). Interestingly, a rhombus-shaped cube with a size of 10 × 10 × 4 mm^3 (10 layers) was also printed by shifting 0.5 mm diagonally when depositing each layer, where no deformation was observed, indicating its structural integrity and fidelity (Fig. 4E). Moreover, a diagonal square with a size of 10 × 10 × 2 mm^3 (5 layers, wall thickness = 0.8 mm) (Fig. 4F, G), a thin-walled tube with a height of 6.4 mm (16 layers, wall thickness = 0.4 mm, diameter = 8 mm) (Fig. 4H, I), and a cone-shaped tube (16 layers, wall thickness = 0.4 mm) with varying diameters along the height of 3–8 mm (Fig. 4J, K **and** Movie S4) were successfully bioprinted as well. Of note, similar constructs were also successfully bioprinted using 3% and 5% GPG bioinks with comparable structural fidelity to those generated using 4% GPG bioink (Fig. S4). To our best knowledge, there are few reports on direct bioprinting of a single-component bioink formulation in such freeform structures without any molding, especially if the bioink requires crosslinking during the bioprinting process[10, 11]. In particular, our shear-thinning GPG bioinks could self-heal and

Author Manuscript Author Manuscript Author Manuscript Author Manuscript

integrate with the previously deposited layers. Therefore, the bioprinted constructs could maintain the pre-designed structures without deformation to allow for subsequent photocrosslinking. Although a guest-host shear-thinning hydrogel based on functionalized HA has been recently demonstrated for direct 3D bioprinting[15], only simple mesh structures were deposited, and sufficient cell adhesion and spreading could only be realized when RGD peptides were simultaneously incorporated. In addition, recent literature has developed an embedded bioprinting strategy to fabricate freeform structures by direct bioprinting of shear-thinning bioinks into self-healing supporting hydrogels[27], but the procedure is generally complicated and time-consuming, making it less suitable for certain applications.

2.4. Direct bioprinting of cell-laden constructs

Despite the fact that GelMA-based bioinks have been bioprinted into 3D constructs, the respective concentration has been limited to higher than 7%[10, 11, 25], and therefore cell spreading and migration were inhibited due to the highly crosslinked hydrogel network. Moreover, GelMA microfibrous structures have been bioprinted using a microfluidic dual-material strategy[31]. It is however anticipated that, if GelMA hydrogels can be bioprinted at much lower concentrations with high structural integrity and fidelity, it would support cell activities by providing softer microenvironments and thus provide new opportunities for applications in tissue engineering.

Using our strategy for direct bioprinting of the GPG bioinks, cell-laden GelMA constructs with high structural fidelity were obtained by using the bioinks at relatively low concentrations of 3%, 4%, and 5%. To validate the possible use of the GPG bioinks for bioprinting, we first investigated the effect of the cooling process on the cell viability by fabricating 3D constructs with a conventional molding process using the GelMA pre-bioinks (before cooling) and the GPG bioinks (after cooling). Specifically, HUVECs with a cell density of 4×10^6 mL^{-1} were adopted to evaluate the bioactivity of the constructs with a 1.6-mm thickness and a 10-mm diameter. Live/Dead staining indicated that the respective viabilities of HUVECs in the constructs made from the GelMA pre-bioinks at concentrations of 3%, 4%, and 5% were 90.7% ± 7.2%, 88.8% ± 5.0%, and 89.9 ± 2.6% (Fig. 5A–C, G). In comparison, the viabilities of HUVECs in the constructs made from the GPG bioinks reached 90.4% ± 2.9%, 84.0% ± 5.6%, and 84.0% ± 6.2%, respectively (Fig. 5D–G). These results indicated that the cooling of the GelMA pre-bioinks to their respective GPG bioinks did not exert noticeable negative impact on the viability of the encapsulated HUVECs.

We then investigated the effect of the extrusion process on the cell viability by bioprinting the GPG bioinks into 3D constructs with a size of $5 \times 5 \times 1.6$ mm^3. When a 27G straight nozzle was used for bioprinting, the viabilities of HUVECs in the bioprinted constructs at day 1 were 75.1% ± 5.2%, 73.7% ± 3.5%, and 69.0% ± 3.1% for the GPG bioinks at concentrations of 3%, 4%, and 5%, respectively (Fig. 6A–C, G). By switching to a cone-shaped nozzle, the cell viabilities were successfully elevated to 88.7% ± 4.1%, 85.8 ± 5.3%, and 85.1 ± 7. at day 1(Fig. 6D–G) and 91.0% ± 3.2%, 90.3% ± 2.9%, and 89.3% ± 0.6% at day 7 (Fig. 6G), respectively. To understand the force experienced by the cells during bioprinting, we further obtained shear stress distribution for the straight and cone-shaped

Author Manuscript Author Manuscript Author Manuscript Author Manuscript

nozzles at each concentration of the GPG bioinks using CFD simulation. The use of a straight nozzle would generate high shear stresses along the entire nozzle length, which averaged to approximately 26 Pa, 115 Pa, and 183 Pa for the GPG bioinks at concentrations of 3%, 4%, and 5%, respectively (Fig. 6H–J, N). In comparison, when a cone-shaped nozzle was employed instead, the high shear stresses only existed at the very tip, which averaged to approximately 23 Pa, 104 Pa, and 174 Pa for GPG bioinks at concentrations of 3%, 4%, and 5%, respectively (Fig. 6K–L, O). Therefore, the lower shear stress that the cells experienced in the cone-shaped nozzle during the bioprinting process should have contributed to the higher cell viabilities comparing to when the straight nozzle was used, for bioinks at all concentrations. Our results are in good agreement with reported studies considering the effect of shear force on cell viability[32].

The pore structures of the bioprinted constructs was further investigated by SEM. When the concentration of the GPG bioinks was raised from 3% to 4% and 5%, the pore diameter of the bioprinted constructs decreased from 135.7 ± 37.3 μm to 66.7 ± 13.8 μm and 49.9 ± 15.1 μm, respectively (Fig. 7A–C, G). On the contrary, the Young's modulus increased from 1.8 ± 0.1 kPa to 3.6 ± 0.2 kPa and 6.9 ± 0.1 kPa, respectively (Fig. 4C). These results indicated that lower concentrations of the GPG bioinks endowed the constructs with larger pores and less stiffness. Furthermore, confocal images confirmed that much better spreading of HUVECs could be observed across the thickness of the bioprinted constructs at lower concentrations of the GPG bioinks (Fig. 7D–F **and** Movie S5). The spreading area of the cells in the constructs bioprinted from 3% GPG bioink, calculated by the occupied area (%) of the cells at day 7, was approximately 20.6% ± 1.6%, which was 4 times and 12 times more than those bioprinted from the 4% and 5% GPG bioinks, respectively (Fig. 7H). In addition, the proliferation of the HUVECs measured by their metabolic activities increased over the 7-day culture period, and the constructs bioprinted from the 3% GPG bioink showed much faster proliferation of the cells than the other constructs at higher concentrations of the GPG bioinks (Fig. 7I). Overall, the constructs bioprinted with the GPG bioinks at lower concentrations featuring higher porosity and lower stiffness enabled better cell activities, especially for cells such as HUVECs that prefer softer substrates[33]. These results could hardly be achieved using current strategies that are limited to a minimum concentration of 7% of GelMA in the bioink[10, 11, 25]. Therefore, the development of the GPG bioinks could lead to successful bioprinting of cell-laden constructs with high structural fidelity and enhanced bioactivity due to the capability to use low concentrations of hydrogels, which have hardly been achieved using conventional single bioinks[4, 10, 19].

To this end, we have demonstrated a promising strategy for direct bioprinting of soft and highly porous constructs of pure GelMA that allowed for enhanced cell activities. It should be noted that, the mechanics of the microenvironments are critical for cell functions, and ideally they should match those of the target tissues to be generated[34]. This requirement becomes particularly important when stem cells are involved, since the differentiation of stem cells is strongly dependent on the stiffness of their substrates, either planar[35] or in 3D[36]. It should be noted that, GPGs could not form anymore at 21 °C when the concentration was decreased to lower than 3%, and thus 3% was the lowest concentration that the GPG bioinks could be bioprinted at this temperature. Such concentration of GPG

Author Manuscript Author Manuscript Author Manuscript Author Manuscript

resulted in a modulus of ~1.8 kPa, close to the ranges that the microenvironments of the brain possess[35], potentially enabling the use of these bioinks for neural tissue engineering. In addition, the concentration of the GPG bioinks (and thus stiffness) may be further decreased by lowering the ambient bioprinting temperature to a level that it allows maintenance of gelation while not affecting the cell viability. Therefore, the ability to fabricate cell-favorable constructs featuring soft tissue-matching low stiffness is an essential advantage of our bioprinting strategy.

It should be noted however, the resolution of the bioprinting demonstrated in this work was limited to approximately 500 μm due to the sizes of nozzles used, which could potentially be improved by using those with smaller dimensions and further fine-tuning of extrusion parameters. More importantly, the GPG bioinks are compatible with the multi-material bioprinting technique that we recently developed[37], making it possible to bioprint heterogeneous tissues using pure GelMA hydrogels to mimic the complex multi-component structure and mechanical heterogeneity of natural tissues. The bioprinted biomimetic tissue constructs using our unique GPG bioink formulations may find widespread applications for use in tissue regeneration and pharmaceutical screening.

3. Conclusions

We have developed a new strategy to enable direct bioprinting of 3D cell-laden GelMA constructs with high structural fidelity and favorable biological properties. The development and employment of the GPG bioinks allowed us to bioprint GelMA constructs at relatively low concentrations of the bioinks (down to 3%, compressive modulus: 1.8 kPa) owing to their shear-thinning and self-healing properties. We showed the structural fidelity by bioprinting the GPG bioinks into various 3D constructs including a rhombus, a thin-walled tube, and a cone-shaped tube, all of which have not been possible to bioprint using conventional bioinks due to gravity. Particularly, the constructs bioprinted from low concentrations of the GPG bioinks with high porosity and low stiffness could effectively support cell survival and enhance cell proliferation as well as spreading, comparing to those at higher concentrations. Moreover, the biological properties of the GPG bioinks may be further improved by incorporating additional bioactive components such as collagens and fibrin. We believe that with further development, our strategy will benefit various applications including tissue engineering, regenerative medicine, and pharmaceutical screening by providing a reliable means for fabricating 3D cell-laden constructs.

4. Experimental Section

Materials

Gelatin, methacrylic anhydride, and 2-hydroxy-4’-(2-hydroxyethoxy)-2-methylpropiophenone (photoinitiator, PI) were purchased from Sigma-Aldrich (St. Louis, MO, USA). GelMA molecules were synthesized according to our previously published protocol[23, 28], at a high degree of methacryloyl substitution (81.4 ± 0.4%). Cell analysis reagents including Live/Dead kit, PrestoBlue, Alexa 488-phalloidin, and 4’,6-diamidino-2-phenylindole (DAPI) were purchased from ThermoFisher (Waltham, MA, USA). All reagents were used without further purification.

Author Manuscript Author Manuscript Author Manuscript Author Manuscript

Preparation of the GPG bioinks

GelMA solutions at 3%, 4%, and 5% containing 25 mM 4-(2-hydroxyethyl)-1-piperazineethanesulfonic acid (HEPES, Sigma-Aldrich), 10% fetal bovine serum (FBS, ThermoFisher), 0.5% PI, and 1% penicillin-streptomycin (P/S, ThermoFisher) were used for the entire studies. The GPG bioinks were obtained by cooling GelMA solutions at 4 °C for approximately 20 min. It should be noted that the GelMA and PI concentrations were calculated by w/v (i.e., g mL^{-1}), while those of FBS and P/S were calculated by v/v. Prior to bioprinting, the GelMA solution was transferred to a 3-mL syringe before the cooling process. For the bioprinting of cell-laden constructs, GelMA solution was mixed with cells before the cooling process. The cell density used for bioprinting was 4×10^6 mL^{-1}.

Bioprinting

The 3D bioprinter was modified from a commercial 3D printer (Lulzbot TAZ 4, Aleph Objects, Loveland, CO, USA) by replacing the pre-installed printhead with a syringe pump in a way that it did not interfere with the movement of the printer but allowed precise deposition of the bioink. All the bioprinting was conducted at 21 °C. The printing speed was kept constant at 400 mm min^{-1}. Unless otherwise noted, the bioprinted constructs were always further UV-crosslinked for 30 s at a power of 3.95 W cm^{-2} (OmniCure S2000, Excelitas Technologies, Waltham, MA, USA) immediately after bioprinting to obtain permanent structures.

Characterization of the bioinks

The gelation kinetics was studied by measuring the evolution of storage (G') and loss modulus (G") using a rheometer (AR-G2, TA Instruments, New Castle, DE, USA) with a 40-mm diameter, 2° cone plate geometry, and 54-μm plate-to-plate distance. The mechanical spectra were obtained at a constant strain of 5% in a frequency range of 0.1–100 rad s^{-1} at 21 °C, and conducted immediately after two sequential processes of cooling (4 °C, 5 min) and recovery (21 °C, 5 min). The temperature dependence of G' and G" were obtained using temperature sweep (oscillation) by decreasing temperature from 37 °C to 2 °C at a cooling rate of 5 °C min^{-1}, while the time dependence of G' and G" were determined by time sweep (oscillation) at 4 °C and 21 °C, respectively (the frequency and shear strain were maintained constant at 10 rad s^{-1} and 5%, respectively). To study the stability of the GPG bioinks, the G', G", and viscosity measurements as a function of time (0–20 min) were obtained at 21 °C immediately after cooling the samples at 4 °C for 5 min. The viscosity measurements as a function of shear rate (0–100 s^{-1}) were conducted at 21 °C immediately after two sequential processes of cooling (4 °C, 5 min) and recovery (21 °C, 5 min).

The gelation time was investigated at 4 °C and 21 °C by recording the videos when the samples (5 mL) were fastened on a standard analog shaker, and determined when the solutions stopped shaking. To ensure that the starting temperatures of the samples were the same, the samples were maintained at 37 °C for at least 20 min before the measurements.

In addition, the mechanical properties of the GPG bioinks before and after UV crosslinking were measured by compression tests using a mechanical testing machine at 21 °C (Instron 5943, Instron, Norwood, MA, USA).

Author Manuscript Author Manuscript Author Manuscript Author Manuscript

Simulations of the GPG bioinks during bioprinting

The bioprinting processes of the GPG bioinks were simulated using computational fluid dynamics (CFD, Fluent, Ansys, Providence, RI, USA) to obtain the shear stress distribution in the straight and cone-shaped nozzles. Both nozzles were constructed as axisymmetric computational geometries. The length and diameter of the straight nozzle were 12 mm and 0.24 mm. The length, input, and output diameters of the cone-shaped nozzle were 50 mm, 5.25 mm, and 0.67 mm, respectively. The feeding rate at the inlet of the nozzles was set as 100 μL min^{-1}. The obtained viscosity data of the GPG bioinks were linked to the computational solver by a user-defined function.

Cell culture

Human umbilical vein endothelial cells (HUVECs, Angio-Proteomie, Boston, MA, USA) were cultured in endothelial growth medium (EGM)-2 supplemented with BulletKit (Lonza, Walkersville, MD, USA) and 1% P/S. Medium was changed every other day. The culture environment was maintained at a 37 °C incubator with 5% humidified atmosphere of CO_2.

Characterization of bioprinted constructs

Scanning electron microscopy (SEM, JSM-5600LV, JEOL, Akishima, Tokyo, Japan) was used to characterize the pore structures of the bioprinted constructs. In order to remove the aqueous phase, the samples were freeze-dried and sputter-coated with gold before imaging. Cell viability was determined by Live/Dead assay according to the manufacturer's protocol (ThermoFisher). In addition, F-actin and nuclei staining (phalloidin/DAPI) were used to visualize the morphology of HUVECs encapsulated within the bioprinted constructs. Cell proliferation was determined by PrestoBlue to measure the metabolic activity. Fluorescence microscopy images were obtained using an inverted fluorescence microscope (Zeiss Axio observer D1, Zeiss, Thornwood, NY, USA) and/or a laser scanning confocal microscope (IX83, Olympus, Shinjuku-ku, Tokyo, Japan).

Statistics

Unpaired t-tests were performed when two groups were compared, while ANOVA followed by a post-hoc test was performed when more than two groups were compared. Statistical analyses were conducted for 3 independent samples per experiment. Statistical significance was determined at a $p<0.05$.

Supplementary Material

Refer to Web version on PubMed Central for supplementary material.

Acknowledgments

The authors acknowledge funding from the National Institutes of Health (AR057837, DE021468, D005865, AR068258, AR066193, EB022403, EB021148) and the Presidential Early Career Award for Scientists and Engineers (PECASE) and the Fundamental Research Funds for the Central Universities from China (No. 14D310106). W.L. acknowledges the financial support from the program of China Scholarships Council (No. 201406630041). Y.S.Z. acknowledges the National Cancer Institute of the National Institutes of Health K99/R00 Pathway to Independence Award (CA201603). A.A. acknowledges the financial support from TUBITAK (No. 1059B191401244).

Author Manuscript Author Manuscript Author Manuscript Author Manuscript

References

1. Zhang B, Montgomery M, Chamberlain MD, Ogawa S, Korolj A, Pahnke A, Wells LA, Massé S, Kim J, Reis L. Nat. Mater. 2016; 15:669. [PubMed: 26950595] Schacht K, Jüngst T, Schweinlin M, Ewald A, Groll J, Scheibel T. Angew. Chem. Int. Ed. 2015; 54:2816.Derby B. Science. 2012; 338:921. [PubMed: 23161993]
2. Murphy SV, Atala A. Nat. Biotechnol. 2014; 32:773. [PubMed: 25093879]
3. Visser J, Melchels FP, Jeon JE, van Bussel EM, Kimpton LS, Byrne HM, Dhert WJ, Dalton PD, Hutmacher DW, Malda J. Nat Commun. 2015; 6Huang ZM, Zhang YZ, Kotaki M, Ramakrishna S. Compos. Sci. Technol. 2003; 63:2223.Li D, Xia Y. Adv. Mater. 2004; 16:1151.Bajaj P, Schweller RM, Khademhosseini A, West JL, Bashir R. Annu Rev Biomed Eng. 2014; 16:247. [PubMed: 24905875]
4. Kang H-W, Lee SJ, Ko IK, Kengla C, Yoo JJ, Atala A. Nat. Biotechnol. 2016; 34:312. [PubMed: 26878319]
5. Tumbleston JR, Shirvanyants D, Ermoshkin N, Janusziewicz R, Johnson AR, Kelly D, Chen K, Pinschmidt R, Rolland JP, Ermoshkin A. Science. 2015; 347:1349. [PubMed: 25780246] Zhang AP, Qu X, Soman P, Hribar KC, Lee JW, Chen S, He S. Adv. Mater. 2012; 24:4266. [PubMed: 22786787]
6. Gauvin R, Chen Y-C, Lee JW, Soman P, Zorlutuna P, Nichol JW, Bae H, Chen S, Khademhosseini A. Biomaterials. 2012; 33:3824. [PubMed: 22365811]
7. Sheth R, Balesh ER, Zhang YS, Hirsch JA, Khademhosseini A, Oklu R, Vasc J. Interv. Radiol. 2016; 27:859.Zhang YS, Duchamp M, Oklu R, Ellisen LW, Langer R, Khademhosseini A. ACS Biomater Sci Eng. 2016Zhang YS, Yue K, Aleman J, Moghaddam K, Bakht SM, Dell'Erba V, Assawes P, Shin SR, Dokmeci MR, Oklu R, Khademhosseini A. Ann. Biomed. Eng. 2016
8. Chimene D, Lennox KK, Kaunas RR, Gaharwar AK. Ann Biomed Eng. 2016; 44:2090. [PubMed: 27184494] Jungst T, Smolan W, Schacht K, Scheibel T, Groll J. Chem. Rev. 2016; 116:1496. [PubMed: 26492834]
9. Smith CM, Stone AL, Parkhill RL, Stewart RL, Simpkins MW, Kachurin AM, Warren WL, Williams SK. Tissue Eng. 2004; 10:1566. [PubMed: 15588416]
10. Billiet T, Gevaert E, De Schryver T, Cornelissen M, Dubruel P. Biomaterials. 2014; 35:49. [PubMed: 24112804]
11. Luiz EB, Juliana CC, Vijayan M, Ana LC, Nupura SB, Wesleyan AA, Pinar Z, Nihal EV, Amir MG, Mehmet RD, Ali K. Biofabrication. 2014; 6:024105. [PubMed: 24695367]
12. Tamayol A, Najafabadi AH, Aliakbarian B, Arab-Tehrany E, Akbari M, Annabi N, Juncker D, Khademhosseini A. Adv Healthc Mate. 2015; 4:2146.
13. Gao Q, He Y, Fu J-z, Liu A, Ma L. Biomaterials. 2015; 61:203. [PubMed: 26004235] Luo Y, Lode A, Gelinsky M. Adv Healthc Mate. 2013; 2:777.
14. Nakamura M, Iwanaga S, Henmi C, Arai K, Nishiyama Y. Biofabrication. 2010; 2:014110. [PubMed: 20811125]
15. Ouyang L, Highley CB, Rodell CB, Sun W, Burdick JA. ACS Biomater Sci Eng. 2016
16. Bertassoni LE, Cecconi M, Manoharan V, Nikkhah M, Hjortnaes J, Cristino AL, Barabaschi G, Demarchi D, Dokmeci MR, Yang Y, Khademhosseini A. Lab Chip. 2014; 14:2202. [PubMed: 24860845]
17. Cui X, Breitenkamp K, Finn M, Lotz M, D'Lima DD. Tissue Eng Part A. 2012; 18:1304. [PubMed: 22394017]
18. Fedorovich NE, De Wijn JR, Verbout AJ, Alblas J, Dhert WJ. Tissue Eng Part A. 2008; 14:127. [PubMed: 18333811]
19. Kolesky DB, Homan KA, Skylar-Scott MA, Lewis JA. Proc Natl Acad Sci U S A. 2016; 113:3179. [PubMed: 26951646] Kolesky DB, Truby RL, Gladman A, Busbee TA, Homan KA, Lewis JA. Adv. Mater. 2014; 26:3124. [PubMed: 24550124]
20. Jia W, Gungor-Ozkerim PS, Zhang YS, Yue K, Zhu K, Liu W, Pi Q, Byambaa B, Dokmeci MR, Shin SR, Khademhosseini A. Biomaterials. 2016; 106:58. [PubMed: 27552316]

Author Manuscript Author Manuscript Author Manuscript Author Manuscript

21. Carrow JK, Kerativitayanan P, Jaiswal MK, Lokhande G, Gaharwar AK. Essentials of 3D Biofabrication and Translation. 2015; 229Melchels FPW, Domingos MAN, Klein TJ, Malda J, Bartolo PJ, Hutmacher DW. Prog Polym Sci. 2012; 37:1079.
22. Yue K, Trujillo-de Santiago G, Alvarez MM, Tamayol A, Annabi N, Khademhosseini A. Biomaterials. 2015; 73:254. [PubMed: 26414409]
23. Loessner D, Meinert C, Kaemmerer E, Martine LC, Yue K, Levett PA, Klein TJ, Melchels FP, Khademhosseini A, Hutmacher DW. Nat Protoc. 2016; 11:727. [PubMed: 26985572]
24. Soman P, Chung PH, Zhang AP, Chen S. Biotechnol Bioeng. 2013; 110:3038. [PubMed: 23686741] Hribar KC, Soman P, Warner J, Chung P, Chen S. Lab Chip. 2014; 14:268. [PubMed: 24257507]
25. Schuurman W, Levett PA, Pot MW, van Weeren PR, Dhert WJA, Hutmacher DW, Melchels FPW, Klein TJ, Malda J. Macromol Biosci. 2013; 13:551. [PubMed: 23420700]
26. Colosi C, Shin SR, Manoharan V, Massa S, Costantini M, Barbetta A, Dokmeci MR, Dentini M, Khademhosseini A. Adv. Mater. 2015; 28:677. [PubMed: 26606883] Zhu K, Shin SR, van Kempen T, Li YC, Ponraj V, Nasajpour A, Mandla S, Hu N, Liu X, Leijten J. Adv. Funct. Mater. 2017
27. Hinton TJ, Jallerat Q, Palchesko RN, Park JH, Grodzicki MS, Shue H-J, Ramadan MH, Hudson AR, Feinberg AW. Science Adv. 2015; 1:e1500758.Highley CB, Rodell CB, Burdick JA. Adv. Mater. 2015; 27:5075. [PubMed: 26177925] Bhattacharjee T, Zehnder SM, Rowe KG, Jain S, Nixon RM, Sawyer WG, Angelini TE. Science Adv. 2015; 1:e1500655.
28. Nichol JW, Koshy ST, Bae H, Hwang CM, Yamanlar S, Khademhosseini A. Biomaterials. 2010; 31:5536. [PubMed: 20417964]
29. Du Y, Lo E, Ali S, Khademhosseini A. Proc Natl Acad Sci U S A. 2008; 105:9522. [PubMed: 18599452]
30. Djabourov M, Leblond J, Papon P. J Phys. 1988; 49:319.
31. Colosi C, Shin SR, Manoharan V, Massa S, Constantini M, Barbetta A, Dokmeci MR, Dentini M, Khademhosseini A. Adv. Mater. 2015; 28:677. [PubMed: 26606883]
32. Blaeser A, Duarte Campos DF, Puster U, Richtering W, Stevens MM, Fischer H. Adv Healthc Mate. 2016; 5:326.
33. Qi H, Du Y, Wang L, Kaji H, Bae H, Khademhosseini A. Adv. Mater. 2010; 22:5276. [PubMed: 20941801]
34. Discher DE, Janmey P, Wang Y-l. Science. 2005; 310:1139. [PubMed: 16293750]
35. Engler AJ, Sen S, Sweeney HL, Discher DE. 2006; 126:677.
36. Huebsch N, Arany PR, Mao AS, Shvartsman D, Ali OA, Bencherif SA, Rivera-Feliciano J, Mooney DJ. Nat. Mater. 2010; 9:518. [PubMed: 20418863]
37. Liu W, Zhang YS, Heinrich MA, De Ferrari F, Jang HL, Bakht SM, Alvarez MM, Yang J, Li Y-C, Trujillo-de Santiago G, Miri AK, Zhu K, Khoshakhlagh P, Prakash G, Cheng H, Guan X, Zhong Z, Ju J, Zhu GH, Jin X, Shin SR, Dokmeci MR, Khademhosseini A. Adv. Mater. 2017; 29:1604630.

Author Manuscript Author Manuscript Author Manuscript Author Manuscript

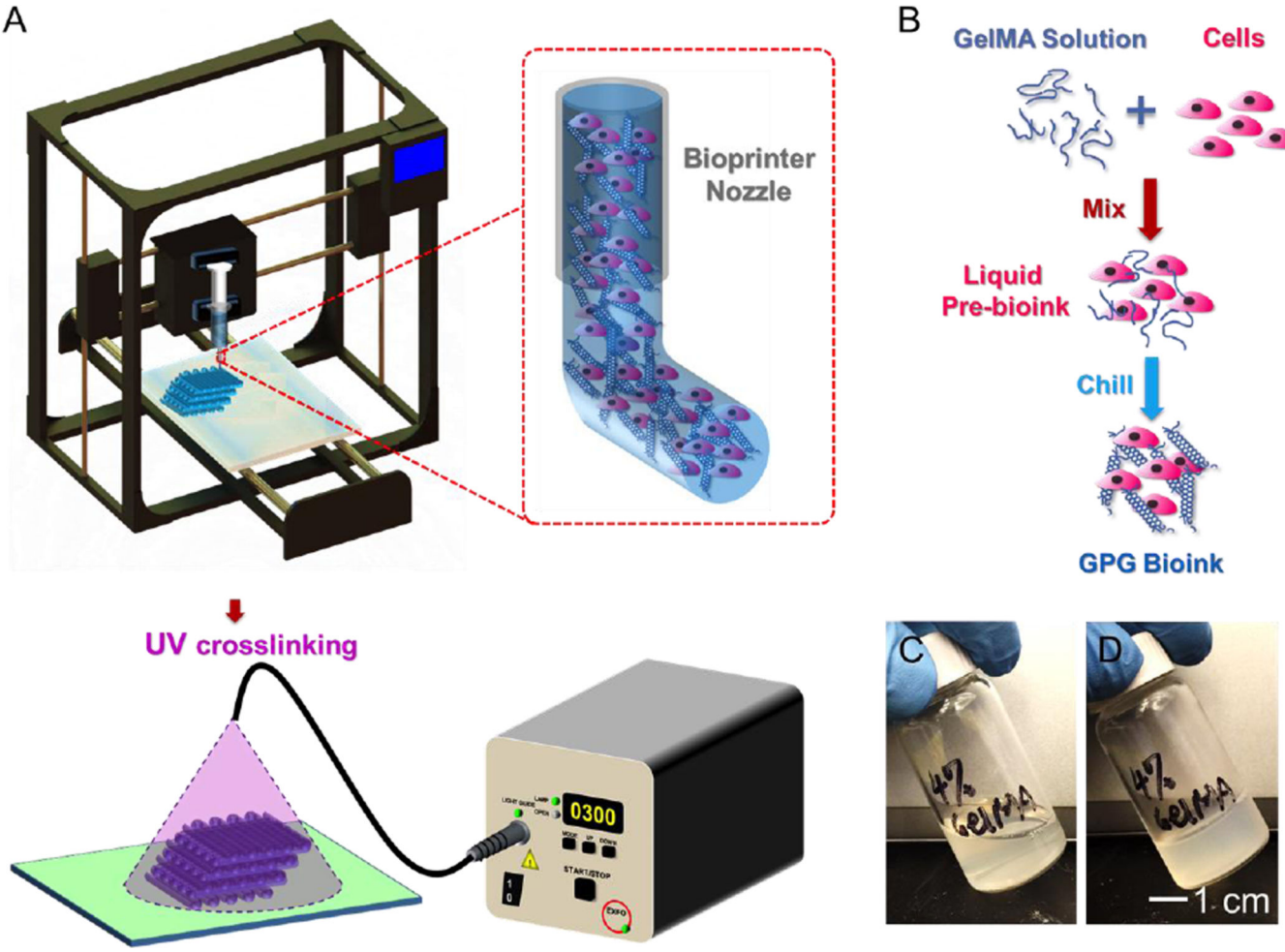

Fig. 1. The strategy of direct bioprinting of the GPG bioinks

A) Schematic diagram showing the deposition of the GPG bioink into predesigned construct which is subsequently photocrosslinked for permanent stabilization. B) Schematic showing the preparation of the GPG bioink by mixing GelMA solution with cells followed by a cooling process to accelerate the gelation process; the GPG bioinks prepared with this strategy possess shear-thinning and self-healing properties and can be directly bioprinted into temporally stable freeform structures with minimal deformation. C, D) Photographs of the 4% GelMA pre-bioink and the corresponding GPG bioink achieved through a cooling process, respectively.

Author Manuscript
Author Manuscript
Author Manuscript
Author Manuscript

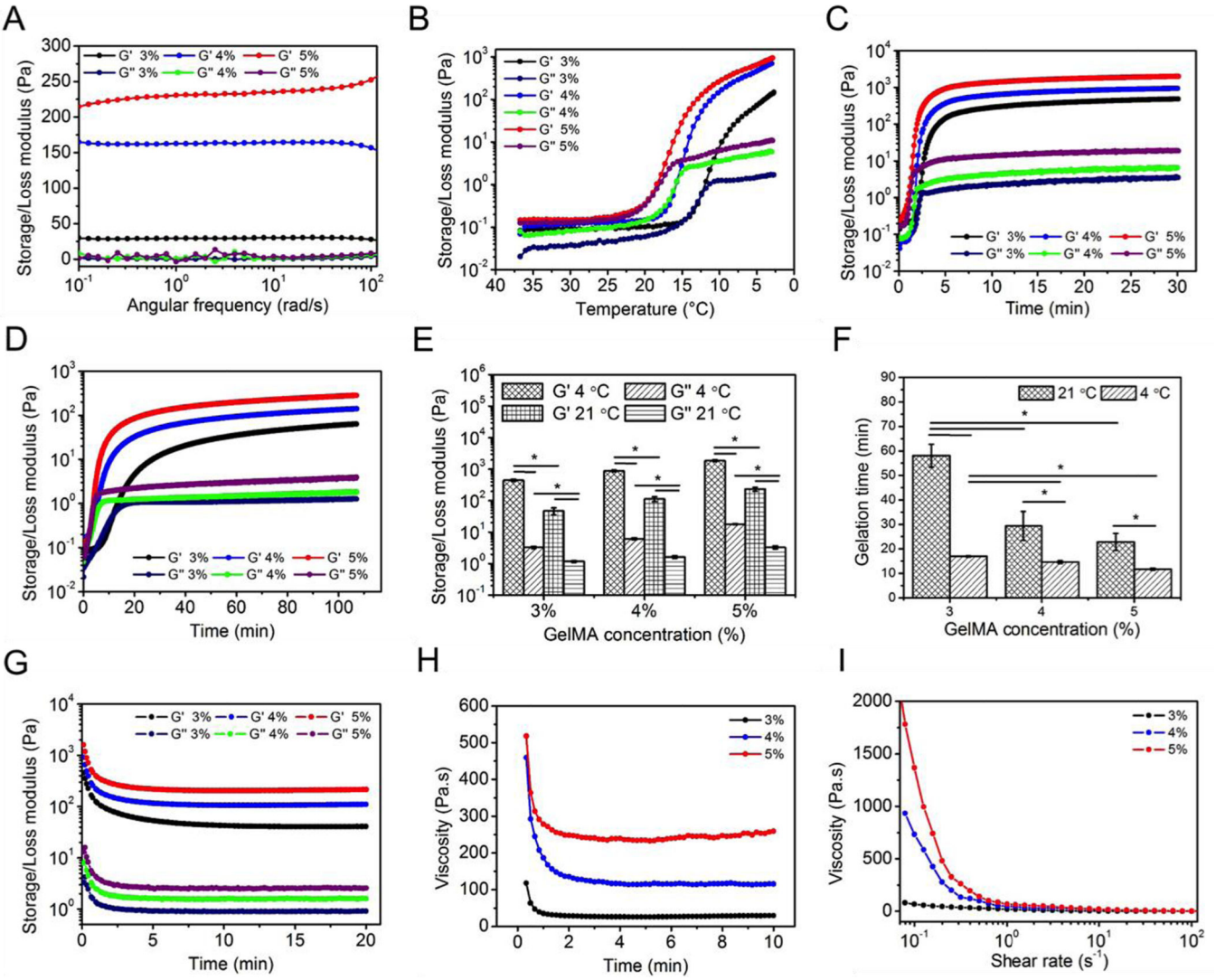

Fig. 2. Characterization of the GPG bioinks

A) Mechanical spectra of the GPG bioinks at 21 °C. B–D) G' and G" values as functions of (B) temperature, (C) time at 4 °C, and (D) time at 21 °C. E) G' and G" values at 4 °C and 21 °C. F) Gelation time at 4 °C and 21 °C. G) G' and G" values as a function of time at 21 °C obtained immediately after cooling the samples at 4 °C for 5 min. H) Viscosity as a function of time at 21 °C obtained immediately after cooling the samples at 4 °C for 5 min. I) Viscosity as a function of shear rate (21 °C).

Author Manuscript Author Manuscript Author Manuscript Author Manuscript

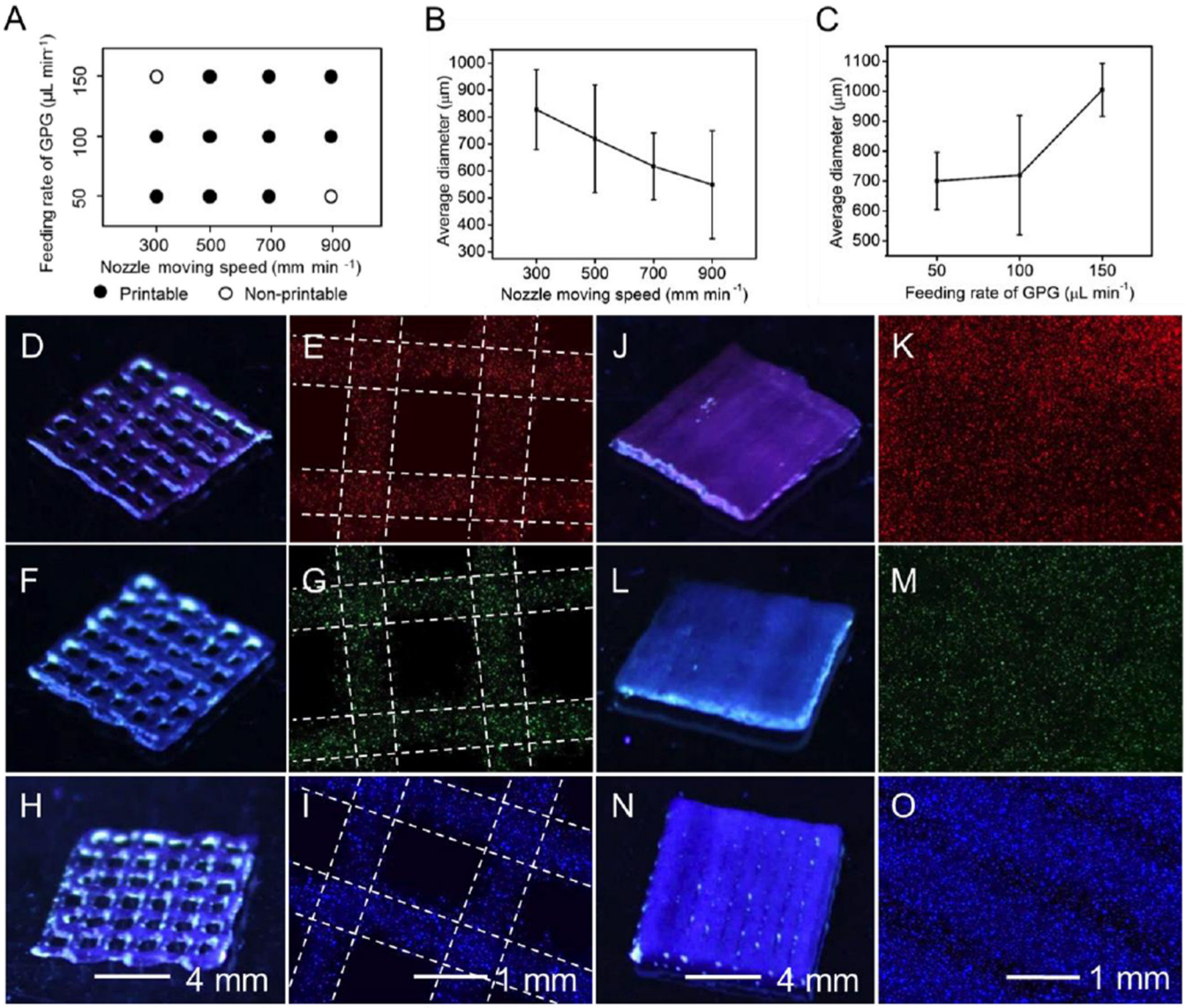

Fig. 3. Printing performance of the GPG bioinks

A) Printability map showing the effect of nozzle moving speed and feeding rate on the printing performance (4% GPG bioink). B, C) the effect of (B) nozzle moving speed and (C) feeding rate of the GPG bioink on the diameter of printed filaments. D–I) Photographs and fluorescence micrographs of bioprinted meshes using (D, E) 3% GPG bioink, (F, G) 4% GPG bioink, and (H, I) 5% GPG bioink. J–O) Photographs and fluorescence micrographs of printed slabs using (J, K) 3% GPG bioink, (L, M) 4% GPG bioink, and (N, O) 5% GPG bioink.

Author Manuscript Author Manuscript Author Manuscript Author Manuscript

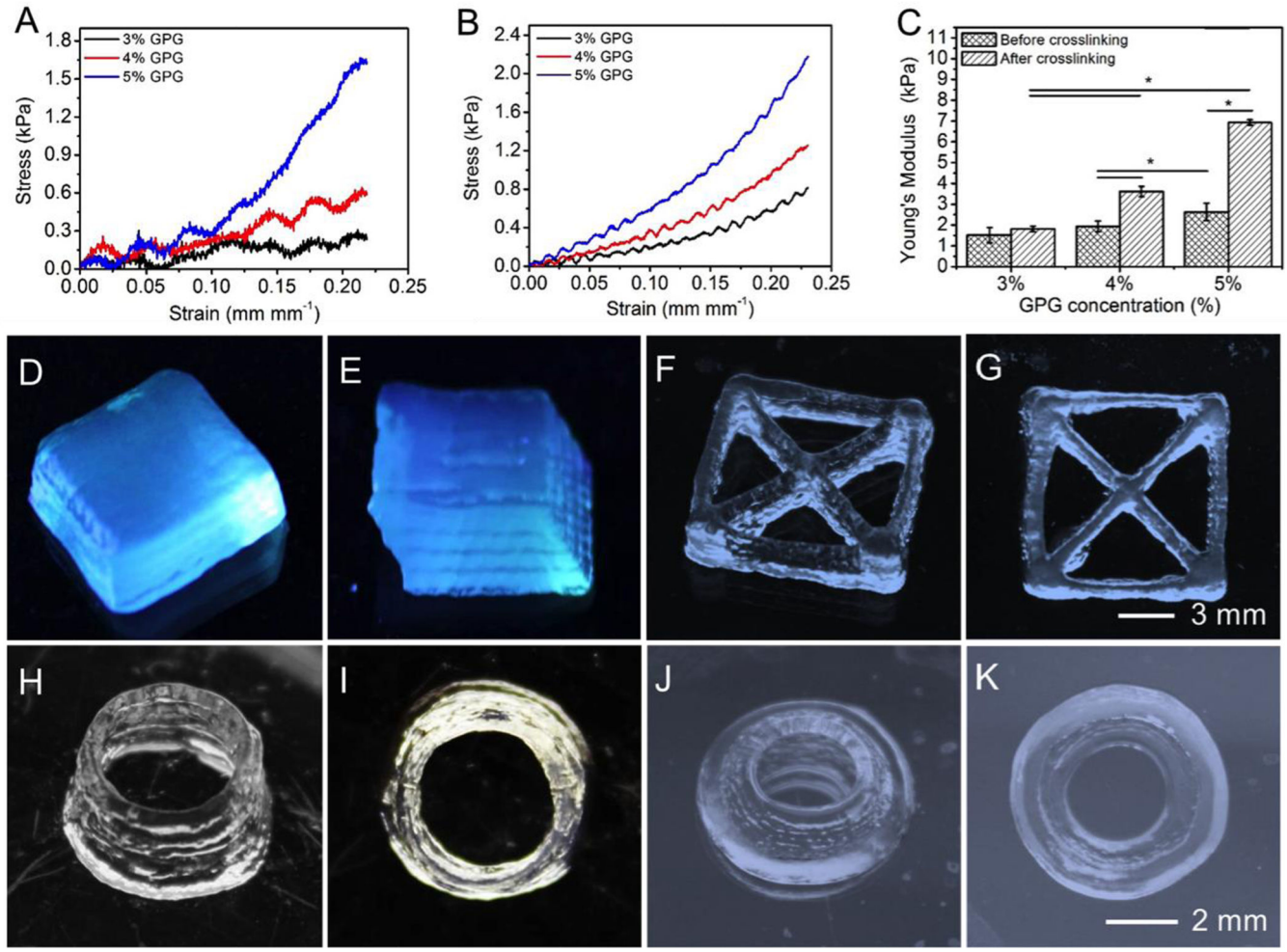

Fig. 4. Direct bioprinting of 3D constructs using the GPG bioinks

A, B) Stress-strain curves of the bioprinted constructs (A) before photocrosslinking and (B) after photocrosslinking. C) Young's modulus of the bioprinted constructs. D–K) Photographs showing various bioprinted structures without noticeable deformation (4% GPG bioink), including (D) a cube, (E) a rhombus, (F, G) a diagonal square, (H, I) a thin-walled tube, and (J, K) a cone-shaped tube.

Author Manuscript Author Manuscript Author Manuscript Author Manuscript

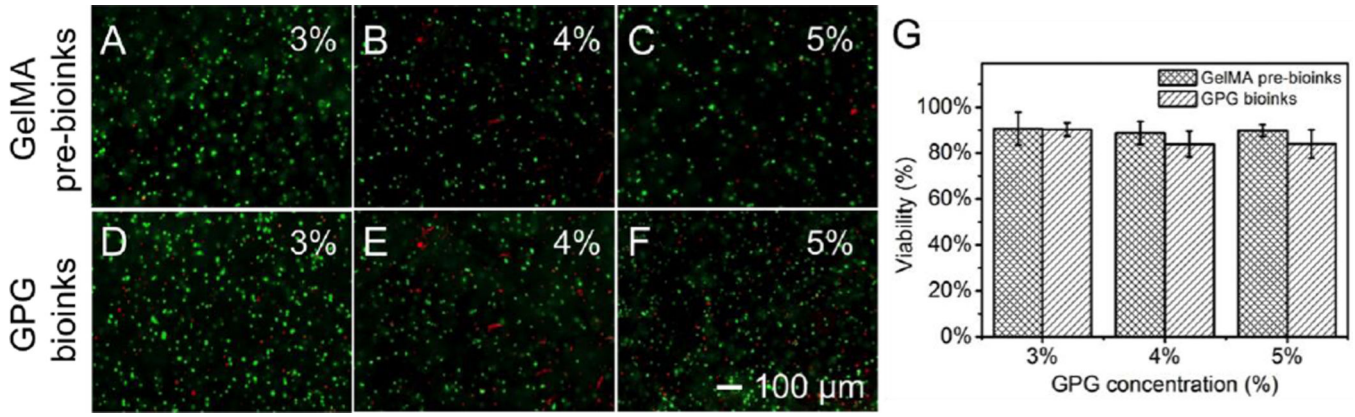

Fig. 5. The effect of cooling process on the cell viability

A–F) Live/Dead staining (day 1) of constructs fabricated with a conventional molding process using (A–C) the GelMA pre-bioinks and (D–F) the GPG bioinks cooled at 4 °C in the presence of cells for approximately 20 min. G) Quantification of viability.

Author Manuscript Author Manuscript Author Manuscript Author Manuscript

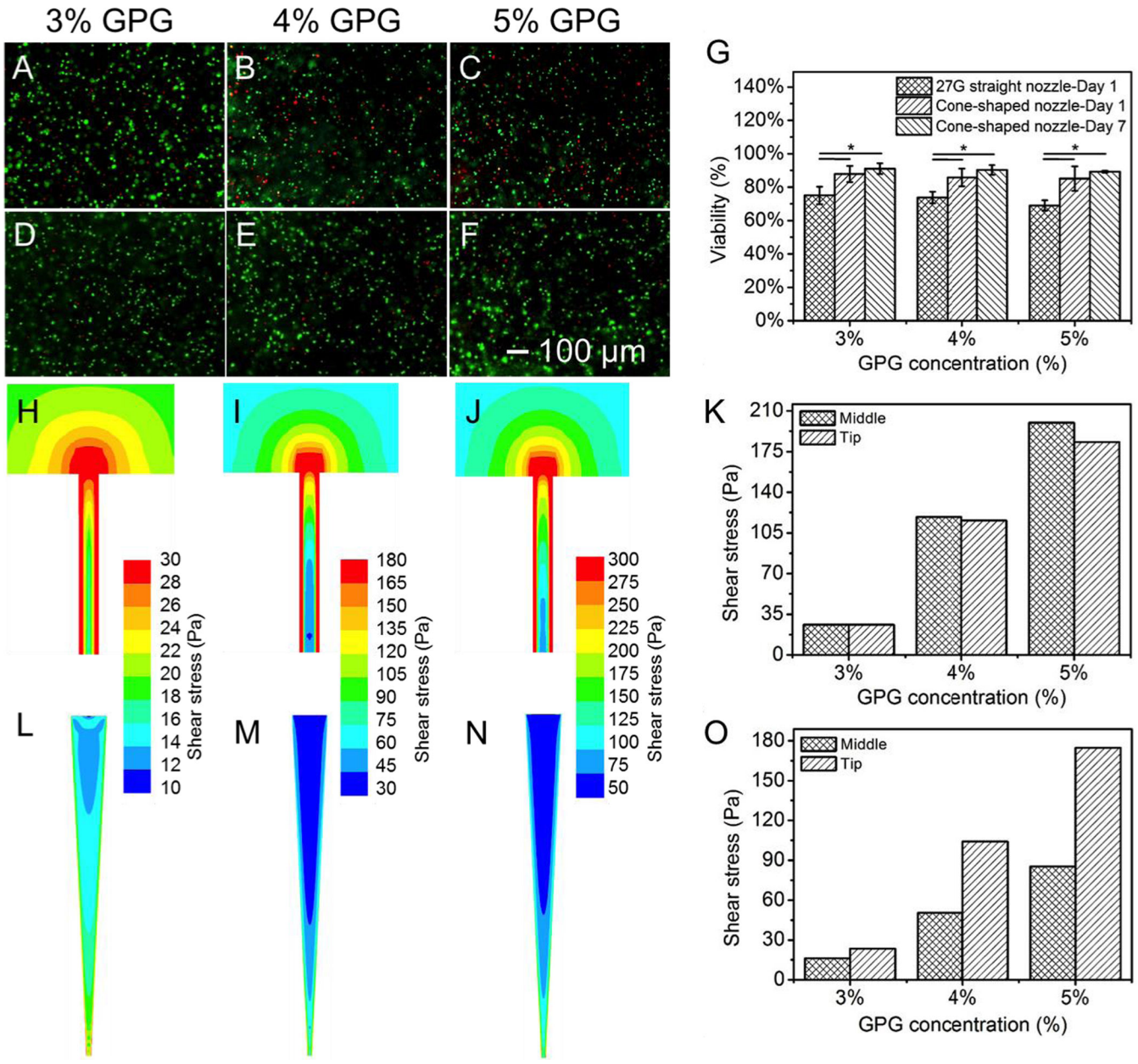

Fig. 6. The effect of the bioprinting process on cell viability

A–F) Live/Dead staining (day 1) of the cell-laden constructs bioprinted using (A–C) a 27G straight nozzle (length = 12 mm, inner diameter = 0.24 mm) and (D–F) a cone-shaped nozzle (length = 50 mm, input inner diameter = 5.25 mm, output inner diameter = 0.67 mm). G) Quantification of the cell viability. H–M) Shear stress distribution maps during the bioprinting process at the feeding rate of 100 μL min^{-1} using (H–J) a 27G straight nozzle and (K–M) a cone-shaped nozzle. N, O) Quantification of shear stress at the middle and tip of (N) the 27G straight nozzle and (O) the cone-shaped nozzle.

Author Manuscript Author Manuscript Author Manuscript Author Manuscript

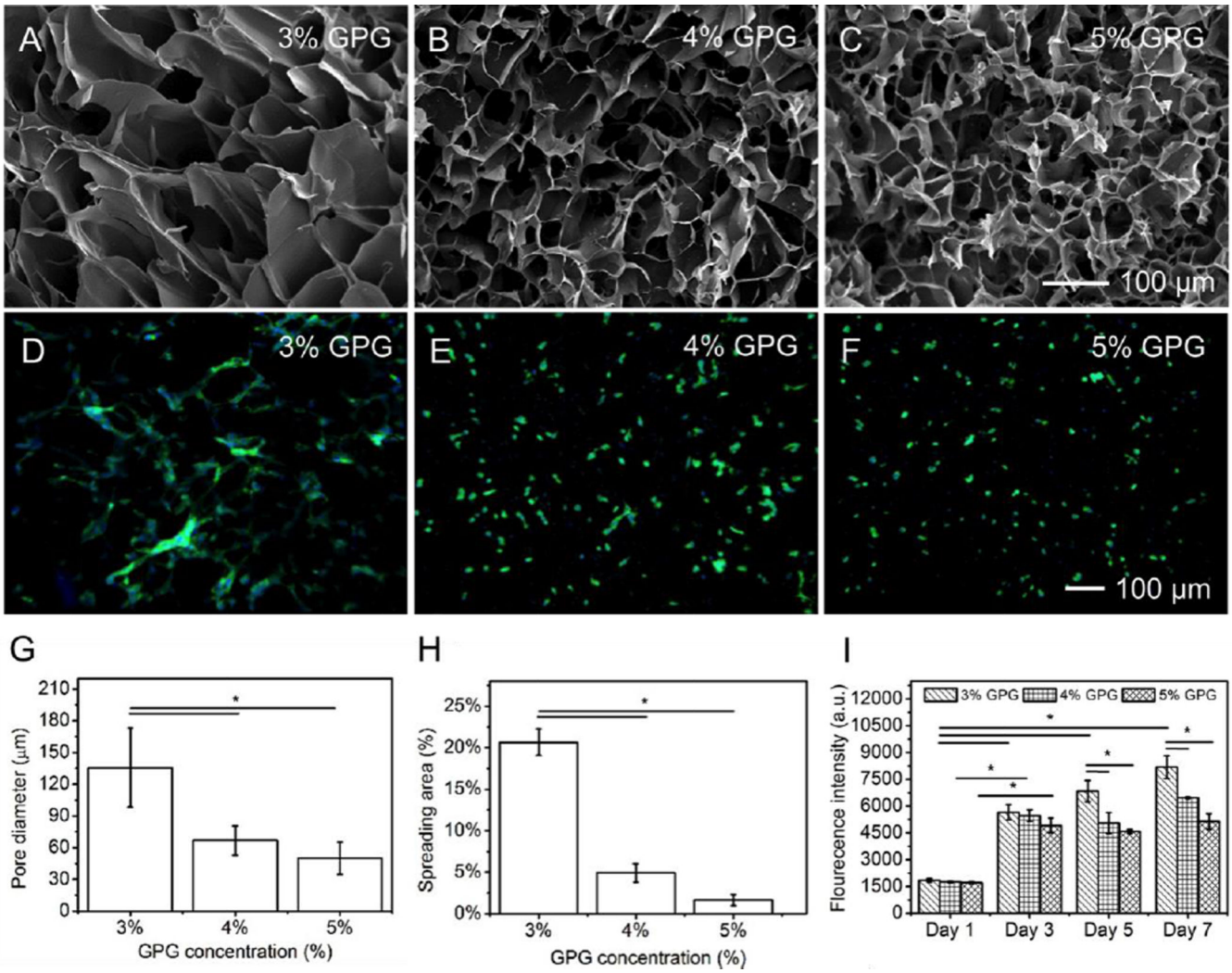

Fig. 7. Direct bioprinting of 3D cell-laden constructs using the GPG bioinks

A–C) SEM images of bioprinted constructs after freeze-drying showing their porosities. D–F) Fluorescence micrographs showing HUVECs stained for F-actin and nuclei in the bioprinted constructs at day 7. G) Quantification of pore sizes of the bioprinted cell-laden constructs. H) Quantification of spreading areas of HUVECs in the bioprinted constructs at day 7, expressed as percentages of cell areas to those of the entire images. I) Quantification of proliferation of the cells over the 7-day period.